Journal of Wind and Engineering, Vol. 6, No. 2, July 2009, pp. 1-18

SHAPE EFFECTS ON THE WIND-INDUCED RESPONSE OF HIGH-RISE BUILDINGS

Ryan Merrick[1] and Girma Bitsuamlak[2]

[1] Technical Coordinator, RWDI Inc., Guelph, Ontario, Canada, email: Ryan.Merrick@rwdi.com
[2] Assistant professor, Department of Civil and Environmental Engineering/International Hurricane Research Center, Florida International University, Miami, Florida, 33174, email: bitsuamg@fiu.edu

ABSTRACT

This paper explored the effect of building shape on the wind-induced response of a structure through a comprehensive investigation of wind tunnel studies performed at Rowan Williams Davies and Irwin, Inc. (RWDI). The study focused on buildings with foot prints of square, circular, triangular, rectangular and elliptical shapes. Seed buildings were selected from an inventory of structures previously tested in a low-speed boundary layer wind tunnel (BLWT). The measured wind tunnel data for each of the sample seeds were factored to match a representative building shape at full scale for comparison purposes. Load patterns attributed to the cross-sectional shape of the structure were observed in the results. To provide a baseline value for the wind loads, the computed responses for the seeds were compared against the values given by the 2005 National Building Code of Canada (NBCC) and the American Society of Civil Engineers (ASCE) 7-05 Standard. The base load comparisons illustrated how certain building shapes perform in wind events.

Key words: shape effects, bluff bodies, base loads, tall buildings, wind performance, boundary layer wind tunnel

INTRODUCTION

Bluff body aerodynamics plays a critical role in the determination of the principal response of a high-rise building. Tall buildings can be susceptible to excessive motion during wind events that can cause occupant discomfort and reduce the overall appeal of the structure (Kareem, 1992). Furthermore, these excessive motions can create high base loads, which can increase the cost of the structure. Structural engineers generally opt for optimizing the structural system or increasing modal mass to reduce wind-induced motion, as discussed by Kareem (1983). Building motions can also be mitigated by supplemental damping systems, as explained by Brazil et al. (2006) and Breukelman and Haskett (2001). However, consideration of building shape can also lead to improved wind performance (Irwin 2008, and Irwin et al. 1998). This study looked to identify general wind loading patterns for common building shapes, with the objective of encouraging designers to consider bluff body aerodynamics early in the design process.

Shape effects, from a wind engineering perspective, have been investigated by Davenport (1971), via aerodynamic model tests. Hayashida and Iwasa (1990) also examined shape effects on super tall building using rigid models. Corner modifications and their impact on aerodynamic forces were studied in detail by Dutton and Isyumov (1990), Kawai (1998) and Tamura and Miyagi (1999). The present study looks to expand on and support past research, by examining the wind loading patterns on various shapes on a direction by direction basis. The computed wind loads are also benchmarked against two international building standards, the NBCC 2005 and the ASCE 7-2005.

Zhou et al. (2003) provided a novel approach to give designers the necessary knowledge to effectively design structures for wind performance. The respective authors compiled a database of high-frequency base balance (HFBB) test data for structures of various heights and footprints. By inputting key building parameters, designers are provided with an estimate of the wind response of the structure. Our research is intended to supplement the information presented by Zhou et al. (2003), and demonstrate general wind loading patterns for common building shapes. Zhou et al. (2003) suggested that loading data accumulated via commercial wind tunnels tests of buildings in their actual surroundings could be used to supplement an overall loading database. It is encouraging to see the use of such databases for preliminary design purposes included i the commentaries of ASCE 7-05 such as *http://aerodata.ce.nd.edu/interface/ interface.html*

The present study further strengthens this approach by utilizing aerodynamic model studies for actual buildings using high-frequency force balance (HFFB) method conducted by the RWDI group of companies. The HFFB method is a commonly used technique in determining the wind-induced response of tall building. The method, also referred to as the high-frequency base balance, was originally developed by Tschanz and Davenport (1983), and has been in practice for many years as a cost effective way of measuring wind induced loads. The HFFB methodology includes collecting a time history of the base loads (shear forces, bending moments and torsion) on a scaled aerodynamic model in a boundary layer wind tunnel. The rigid aerodynamic model is mounted on a special six degree-of-freedom load cell to measure the base loads, while the inertial loads are evaluated analytically. The dynamic loads and computed inertial loads are then combined to provide the peak design loads. The basic assumption in HFFB tests is that feedback due to aeroelastic effects (i.e. building motions) is negligible compared to the aerodynamic and inertial forces. As such, reasonable wind-induced responses can be obtained by testing a rigid model in a boundary layer wind tunnel. The scaled aerodynamic model, while replicating the shape of the study building, should be light and rigid to avoid any resonance effects due to model vibration and have a flat spectral response due to high damping. For the present study, aerodynamic models with a resonant frequency in the order of approximately 100 Hz were used. While the time histories of the base loads are scaled appropriately to provide the mean and background loads for the test building at full scale, the resonant components are obtained analytically by solving the equation of motion (Tschanz and Davenport (1983), Boggs and Peterka (1989), Xie and Irwin (1998)). The equation of motion governing the fundamental mode of vibration of a tall structure using generalized coordinates is given by Eq. (1),

$$m^*\ddot{x} + c^*\dot{x} + k^*x = P \;\; m^*\ddot{x} + c^*\dot{x} + k^*x = P \tag{1}$$

where m^* m^* c^* c^* k^*, P and x are the generalized mass, damping, stiffness, load, and response, respectively. These parameters are functions of the structure's mass distribution, m m, mode shape, f, natural frequency, f_o f_o, externally applied load, P, displacement of the structure, x and critical damping ratio, ζ. For a lumped-mass system, these parameters take the following form:

$$m^* = \{f\}^T [m]\{f\}$$
$$k^* = (2\pi f_o)^2 m^*$$
$$c^* = 2\zeta\sqrt{m^* k^*}$$
$$P^*(t) = \{f\}^T \{P\} = \sum P_i f_i$$
$$\{x\} = x(t)\{f\}$$

For buildings having linear mode shapes (i.e. $f_i = z/H$ $f_i = z/H$) the generalized force, which is the right hand side RHS of Eq. (1), is the same as the moment at the base, as shown in Eq. (2),

$$\sum P_i f_i = \frac{1}{H}\sum P_i z_i = \frac{M}{H}\sum P_i f_i = \frac{1}{H}\sum P_i z_i = \frac{M}{H} \tag{2}$$

where H and M are the height and base moment of the building, respectively. Since the wind induced generalized force is known via wind tunnel testing, we can use the structural dynamic properties of the full scale building and assumed damping ratios to solve for the unknowns on the left hand side of Eq. (1). This process is usually carried out in the frequency domain. The power spectral density, $S_{p*}(f)\,S_{p*}(f)$, for the base moment is computed first using Eq. (3). The generalized response load for each mode can be obtained by integrating the area under the spectral density function (Eq. 3), as shown in Eq. (4). The contributions from each mode will be combined by using square root of the sum of the squares (SRSS) method to obtain the total generalized response $s_T^2 s_T^2$. $S(f)S(f)$ represents the mean square spectral density, commonly referred to as the power spectral density (PSD).

$$S_x = \frac{1}{k^{*2}} |\mathrm{H}(f)|^2 \, S_{p*}(f) S_x = \frac{1}{k^{*2}} |\mathrm{H}(f)|^2 \, S_{p*}(f) \tag{3}$$

$$H(f)|^2 = \frac{1}{\left[1 - \left(\frac{f}{f_0}\right)^2\right]^2 + \left(\frac{2zf}{f_0}\right)^2}$$

$$s_x = \frac{1}{k^*}\left(\int_0^\infty |H(f)|^2 \, S_{p*}(f)\,df\right)^{1/2} \quad s_x = \frac{1}{k^*}\left(\int_0^\infty |H(f)|^2 \, S_{p*}(f)\,df\right)^{1/2} \tag{4}$$

The difference between the square of generalized response load, $s_T^2 s_T^2$, and the square of the background load, $s_B^2 s_B^2$, represents the resonant loading contributions. Note that $s_B^2 s_B^2$ can be obtained by integrating the spectral density function, $S_{p*}(f)\,S_{p*}(f)$, of the base moment time history. More details on HFFB background, along with corrections for non-ideal mode shapes and approximate load distribution over the height of the building, can be found in Boggs and Peterka (1989), Xie and Irwin (1998), Chen and Kareem (2005a), and Chen and Kareem (2005b). It is worthy of note that the structural properties of a study building are used only during the analytical procedure. Thus the HFFB wind tunnel data can be re-analyzed for new set of revised structural properties, as required, to generate a new set of wind responses provided that the shape of the building remains similar.

Hundreds of HFFB studies were considered for inclusion in this study. The intent was to show general wind load patterns for various building shapes. Availability of this type of information is believed to aid designers in assessing wind responses at the early design stages. Seed buildings were selected to have simplistic footprints similar to one of the following five shapes: square, circle, triangle, rectangle and ellipse. The test data from each of the sample seeds were modified to account for geometry differences. The modified test data, now matching a common building geometry, were then combined with an assumed set of dynamic properties to determine the wind response. The results allow for comparisons of the general wind loading patterns of the studied shapes.

SHAPE SELECTION

Common building shapes were selected for inclusion in this study. Figure 1 presents a photo of a seed building for each the shapes studied. Sample seeds were sought to have open surroundings to avoid unique project specific wind effects caused by adjacent structures. From the database, four buildings for each of the five basic building footprints considered were identified. Details of the sample seeds, including shape, width, height, aspect ratio and slenderness ratio, are presented in Appendix A (dimensions shown in full scale meters). The study also considered seeds for various Reynold's numbers (Re), which should be acknowledged when considering the results. The variation of Re for the various experiments was limited to ±150,000.

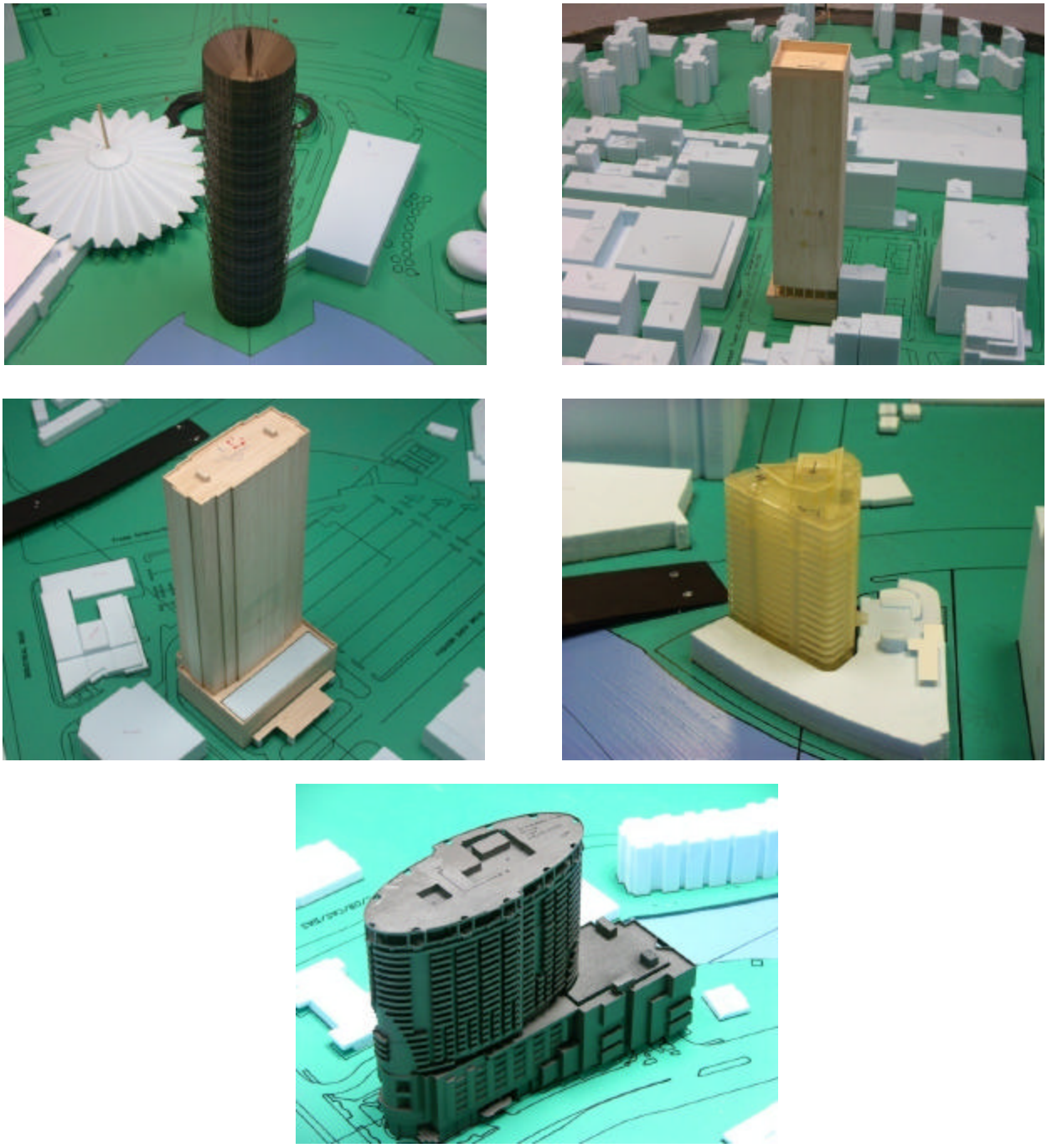

Figure 1. Photos of representative seed buildings.

DATA PROCESSING

Twenty seed buildings were identified for consideration in this research, with four seeds for each of the five study shapes. While the cross-section of each of the seed buildings was similar to one of the five study shapes, the height and width of the seed was varied. In order to compare the data and identify loading trends for particular shapes, it was necessary to normalize the data to represent a common building shape, termed in this paper as representative cylinder. The methodology used to normalize and compute the base loads is discussed in this chapter, while the building and analysis parameters (including the dimensions of the representative cylinders) is discussed in the next section.

The wind loading data from the seed buildings are used to compute the wind loads on the representative cylinders. The data are first reduced into force or moment coefficients using the building shape and test wind speed, and the geometry of the representative cylinder is combined with the moment coefficients to produce the loading on the representative cylinders. The process was repeated for each of the seed buildings, resulting in a set of wind loads that could be compared for each study shape. Eqs. (5) through (9) show the geometric correction factors that were used to convert the seed building loads to be applicable to the geom etry of the representative cylinder.

$$C_{Fx} = \frac{B_{r,x}.h_r.q_{ref}}{B_{s,x}.h_s.q_{ref}} \tag{5}$$

$$C_{Fy} = \frac{B_{r,y}.h_r.q_{ref}}{B_{s,y}.h_s.q_{ref}} \tag{6}$$

$$C_{My} = \frac{B_{r,x}.h_r^{\,2}.q_{ref}}{B_{s,x}.h_s^{\,2}.q_{ref}} \tag{7}$$

$$C_{Mx} = \frac{B_{r,y}.h_r^{\,2}.q_{ref}}{B_{s,y}.h_s^{\,2}.q_{ref}} \tag{8}$$

$$C_{Mz} = \frac{\left(B_{r,x}^{\,2} + B_{r,y}^{\,2}\right).h_R.q_{ref}}{\left(B_{s,x}^{\,2} + B_{s,y}^{\,2}\right).h_R.q_{ref}} \tag{9}$$

In Eqs. (5) through (9), h is the building height; B is the effective width normal to the X or Y axis as indicated; the subscripts s and r denote the seed building and representative cylinder, respectively; and, q_{ref} is the mean velocity pressure at a reference height, taken to be 1.5 m above the floor of the BLWT for all tests (i.e. 600 m at full-scale). These geometric correction factors were applied to the model scale measurements from the BLWT test of each of the seed buildings. The RMS of the base forces and moments for the representative cylinders were computed using the following equation

$$s_{r,i} = s_{s,i} \times C_i$$

where s is the RMS response; C_i is the geometric correction factor for load *i*; the subscript *i* denotes one of $F_xF_x, F_yF_y, M_yM_y, M_xM_x$ or M_zM_z, the subscripts s and r denote the seed building and representative cylinder, respectively. The seed building data was reduced to obtain the non-dimensional PSD in the following form

$$S_{r,i} = \frac{\left(f \times S_{s,i}(f)\right)}{\left(s_{s,i}\right)^2}$$

where *S* is the PSD; and f is the building frequency. The mean and background wind loads on the representative cylinders are computed using the following

$$\overline{R}_{r,i} = \overline{R}_{s,i} \times C_i$$

$$\overline{R}_{r,i} = g_B \times s_{r,i}$$

where, $\tilde{R}\tilde{R}$ and $\hat{R}\hat{R}$ represent the mean, background and resonant wind response. $g_B g_B$ is the background peak factor, typically around 3.5. The resonant wind loads on the representative cylinders were calculated as follows

$$\hat{R}_{r,i} = g_R \times s_{r,i} \times \sqrt{\frac{p \times S_{r,i}(f_1)}{4z_1}}$$

$$g_R = \sqrt{2\ell n(f_1 T)} + \frac{0.5772}{\sqrt{2\ell n(f_1 T)}}$$

where $g_R g_R$ is the resonant peak factor (Tschanz and Davenport, 1983); T is the observation time $f_1 f_1$ is the natural frequency; and, $z_1 z_1$ is critical damping ratio. The peak response of the building, $\hat{R}\hat{R}$, can then be determined by summing the mean loading with the root of the sum of the squares (SRSS) of the background and resonant components, as shown in Eq. (10).

$$\hat{R} = \overline{R} + \sqrt{\tilde{R}^2 + \hat{R}^2}\,\hat{R} = \overline{R} + \sqrt{\tilde{R}^2 + \hat{R}^2} \tag{10}$$

Following this methodology, the resulting wind loads, derived from the seed buildings, correspond to a common geometry and can be compared on a direction by direction basis to identify general wind loads trends on common building shapes.

EXPERIMENT PARAMETERS

The cross-section of each of the seed buildings matched one of the five study shapes, however, the height and width of the seed was varied. The previous section outlined the methodology to normalize the wind loading data collected from the seed buildings to correspond to a representative cylinder of nominal dimensions. The full scale dimensions and coordinate origins for each of the representative cylinders are shown in Figure 2. The height of the representative cylinders were taken to be 150 m at full scale.

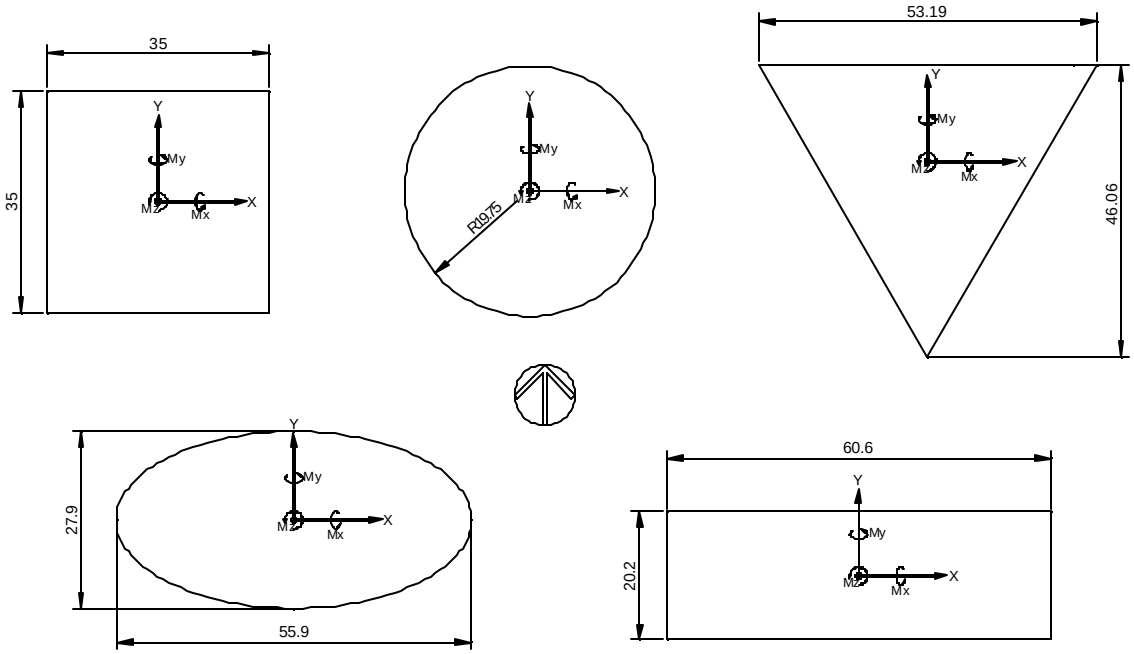

Figure 2. Definition of representative cylinders shapes.

The dimensions shown in Figure 2 were chosen to minimize the geometric correction factors and provide the same cross-sectional area for each representative cylinder. The base overturning moments about *X* and *Y* axis are denoted as M_X and M_Y, respectively. The corresponding base shears along the X and Y axes are denoted throughout this paper as F_x and F_y. The base torsional moment is termed as M_z. The north arrow, in the center of Figure 2, can be used to identify the wind direction. Wind direction is defined as the direction from which the wind blows (commonly referred to as the angle of attack), measured clockwise from north, with north corresponding to 360 degrees.

Assumptions of dynamic properties for the representative cylinders were necessary to permit the computation of the base loads. A building density of 320 kg/m^3 (20 lb/ft^3) was assumed, along with a damping ratio of 2% of critical, which was considered reasonable for strength design of a high-rise structure (Newmark and Hall, 1982). The radius of gyration (R_g) of the structure was estimated as one-third of the diagonal dimension of the representative cylinder. The mass moment of inertia (*MMI*) was then approximated using Eq. (11).

$$MMI = R_g^{\,2} \cdot m \tag{11}$$

In Eq. (11), m indicates the assumed story mass of the representative cylinder. The fundamental natural sway frequencies of the representative structure were approximated based on the height of the building. Table 1 lists the frequencies used in the analysis procedure. For simplicity, only first-order sway and torsion modes were considered. All the three modes were assumed to be linear.

Table 1. Assumed building frequencies.

Cylinder	**Frequency (Hz)**		
	X	Y	Torsion
Square	0.2	0.2	0.4
Circular	0.2	0.2	0.4
Triangular	0.2	0.2	0.4
Rectangular	0.3	0.2	0.4
Elliptical	0.3	0.2	0.4

It should be noted that the present study only looked at a particular configuration of dynamic building properties, as the emphasis was on shape effects. Mass, stiffness and damping levels will no doubt have a significant impact on the loading patterns observed. The effect of these parameters on the general loading patterns of the shapes is discussed in Chan et al. (2009). The impact of mass, stiffness and damping on shape effects is an area that could be examined in future studies in more detail.

The basic design wind speed for the analysis was assumed to be 144 km/hr for 3-second gust at 10 m above ground in open terrain condition. Using the Durst curve for averaging time conversion and the power law for the mean wind speed profile (see Eq. 12), a mean hourly gradient wind speed of 168.5 km/h was calculated.Gradient height was assumed to be 600 m above ground for this investigation.

$$U_g = U_h \cdot \left[\frac{z_g}{z_h} \right]^{0.14} \tag{12}$$

In Eq. (12), *U* and *z* denotes the wind velocity and height above ground, respectively, and the subscripts g and *h* represent gradient height and height of interest, respectively. An open terrain profile, assumed by the exponent in Eq. (12), was used to compute the gradient wind speed. The wind tunnel terrain profile for each of the sample seeds was accounted for via a gust speed correction factor. The wind response of the sample seeds was factored by the ratio of the gust wind speed at the stagnation point during testing of the seeds versus the desired gust speed in an open profile at the stagnation point of the representative cylinder. The resulting factored response gives the wind loading on the representative cylinders.

Wind directionality effects were not considered in this study. Numerous approaches to apply wind direction reductions have been suggested in the literature, but no consensus has been reached (Simiu & Miyata, 2006). Therefore, the results presented in the following sections are the raw base loads and do not account for the probability of extreme winds occurring in each sector.

RESULTS AND DISCUSSION

The wind responses for each of the representative cylinders were derived from the measured seed building data using the methodology and parameters outlined in previous sections. This section presents azimuthal plots of the computed base loads, and indentifies general loading patterns for each of the shapes.

The calculated base loads, on a direction-by direction basis, demonstrate good agreement between the sample seeds. Yet, some variation was observed, which can be expected as the loading data for each of the seeds was retrieved from a distinct wind tunnel test with unique surrounding structures. The authors emphasize that they are in no way recommending the procedure outlined in this paper as a surrogate for wind tunnel testing. It is only hoped that the findings of this research will encourage designers to consider wind performance early in the design process (when the building shape is contrived). Once the design has reached a mature stage, a BLWT study will still be advisable to determine the specific wind response of the structure.

Figure 3 plots the base sway loads for the square cylinder using the factored data for all four seed buildings. Since all of the sample seeds were factored to match the same geometry, they are not distinctly identified in Figure 3. Rather, the peak dynamic loads for each seed are shown by the blue lines and mean loading is identified by the red series. The average of the four seeds is shown with a thick black line, with the uppermost line being the maximum, the lowermost line being the minimum, and the middle line showing the mean wind loading. As a benchmark, the ASCE 7-05 (cyan) and the NBCC 2005 (pink) peak base loads are also included in the plot.

From the sway moment and shear plots in Figure 3, peak lift moments are evident from 180 and 360 for M_y and $S_{x,}$ and from 90^0 and 270^0 for the M_x and S_y loading. These peak loads are caused by vortex shedding, which is identified by the signature high dynamic spikes and zero mean-loading values. The code calculated wind loads from the ASCE 7-05 and NBCC 2005 demonstrate good agreement when estimating the drag moments and shears, but fail to forecast the peak lift loads. Building designers should be aware of this occurrence and investigate methods to remedy the problem, or employ wind testing techniques to quantify the lift loading. The mitigation technique of corner modification was used by Irwin (2008) for the Taipei 101 Tower, and a 25% reduction on the base sway moments was reported. Browne et al. (2005) also discusses the efficiency of balconies located at corners in disrupting the formation of coherent vortices, which is the main source of liftforces.

Figure 4 illustrates the base loads for each wind direction as experienced by the circular cylinder. Again, the computed wind loads from the ASCE 7-05 (cyan) and the 2005 NBCC (pink) are shown.

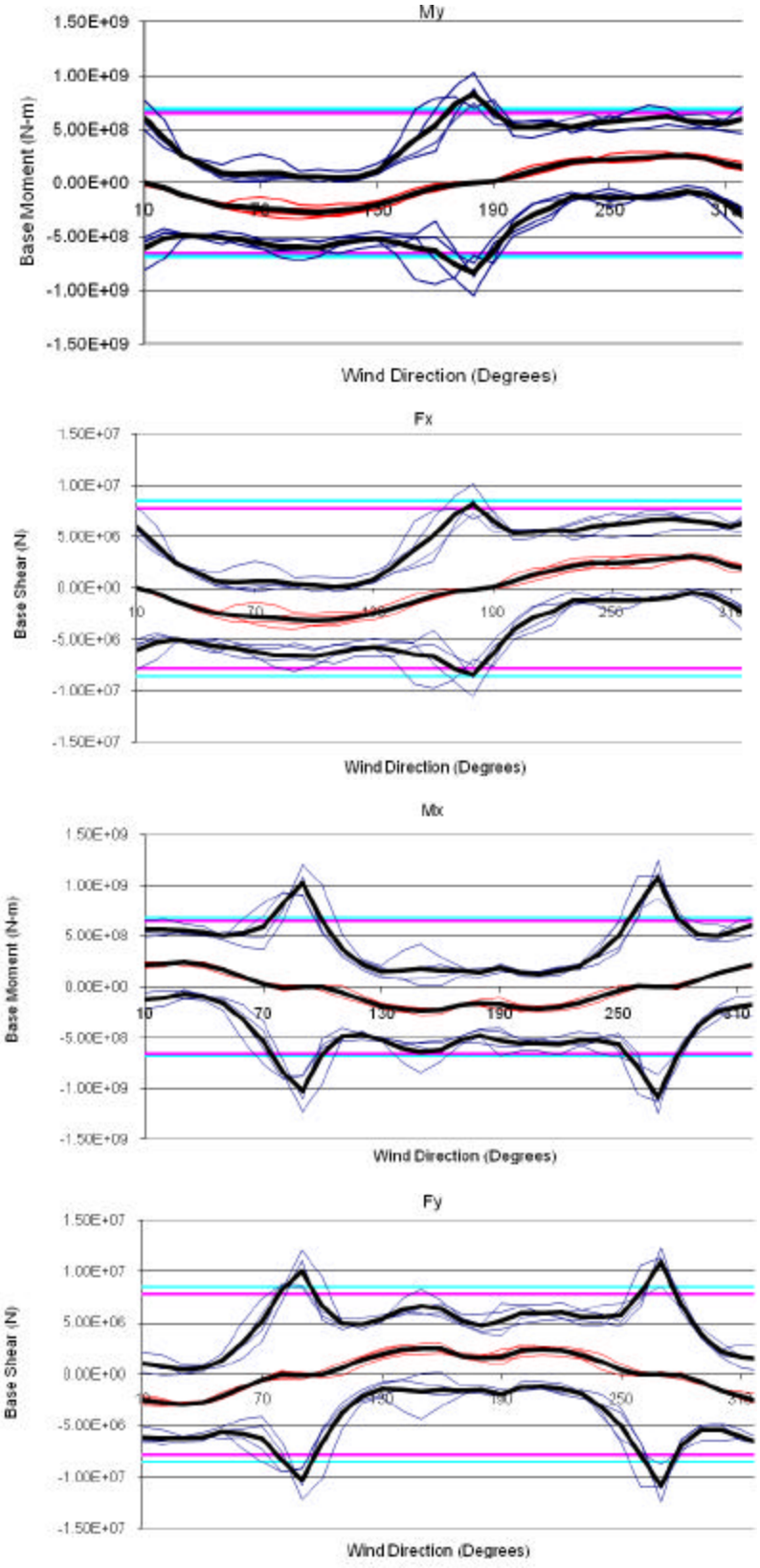

Figure 3. Base moments and shears for square cylinder.

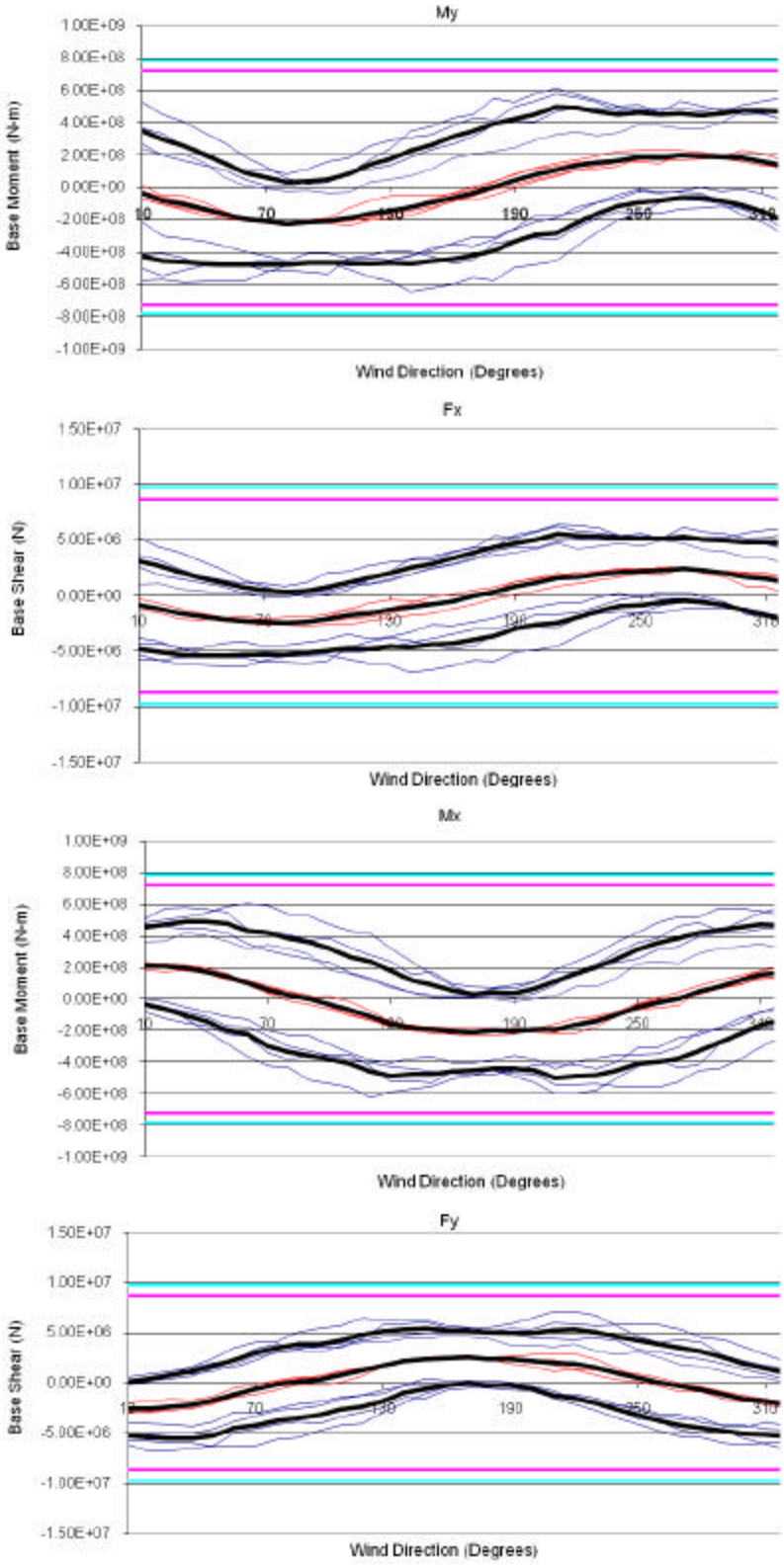

Figure 4. Base moments and shears for circular cylinder.

The code prescribed loads are sufficient in estimating the peak dynamic loads on the circular cylinder, with all of the seeds contained by the estimates. Vortex shedding was not distinctly observed. This was attributed to the fact the sample seeds were generally large radius, rough-walled cylinders capable of producing super-critical Reynolds number flow in the BLWT. For smooth cylindrical structures of smaller radii, such as air traffic control towers or chimney stacks, vortex-induced oscillation may be prevalent as suggested by Jackson (1987) and Simiu and Scanlan (1996).

The base loads of the factored sample seeds for the representative triangular cylinder are provided in Figure 5.

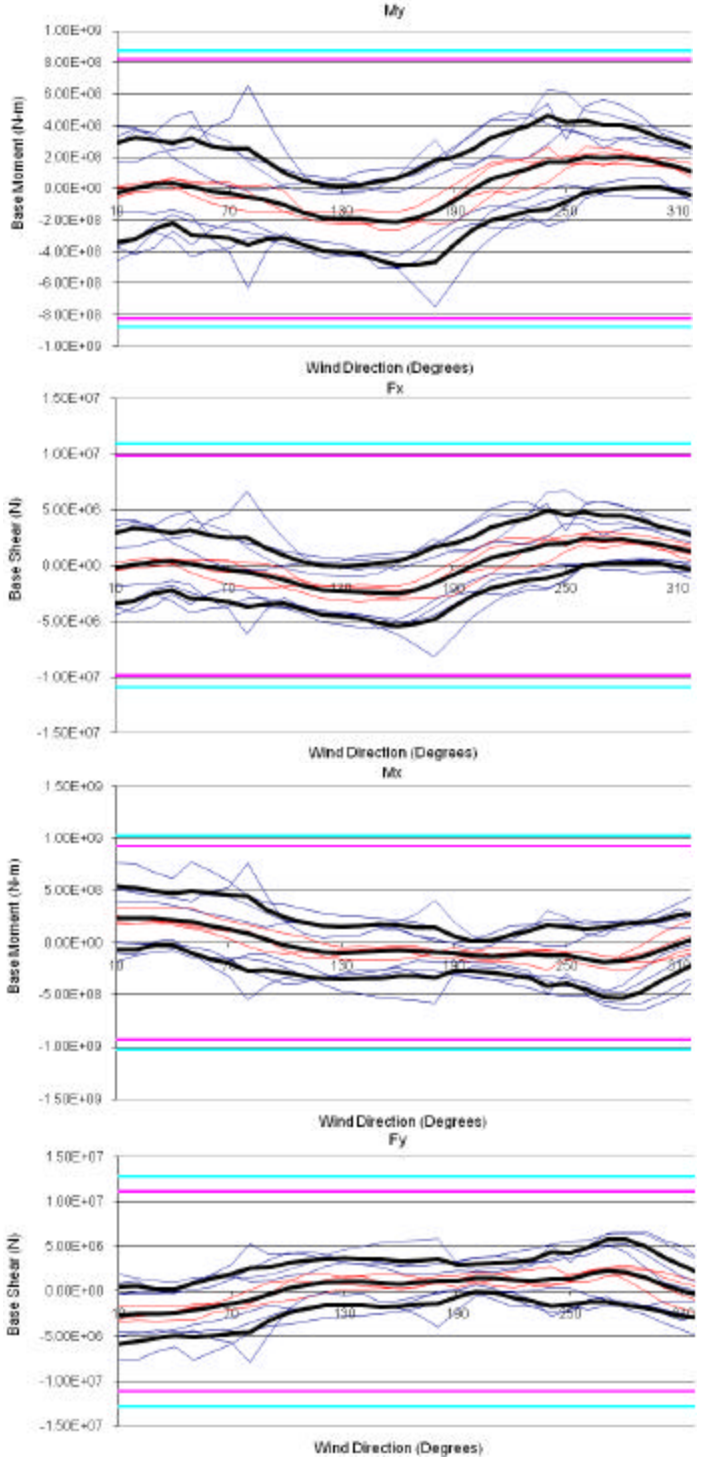

Figure 5. Base moments and shears for triangular cylinder.

All of the computed base loads on the triangular cylinder are less than those computed by building code. This is due to the fact that the code calculation is based on the projected width of the cylinder and does not account for the aerodynamics of the shape. Note that even from wind directions normal to a face of the triangular section, the wind loads are significantly less than the anticipated building code value. Consequently, savings in terms of cost and materials may be available resulting from the application of wind tunnel testing methods versus code provisions for the design of triangular structures. It would also be interesting to investigate the resultant base loads that occur simultaneously on the triangular cylinder, since Figure 5 shows coupling between the X and Y direction forces for wind direction 260 .

Figure 6 depicts the calculated loads at the base of the rectangular cylinder, along with the load estimates derived from the building codes.

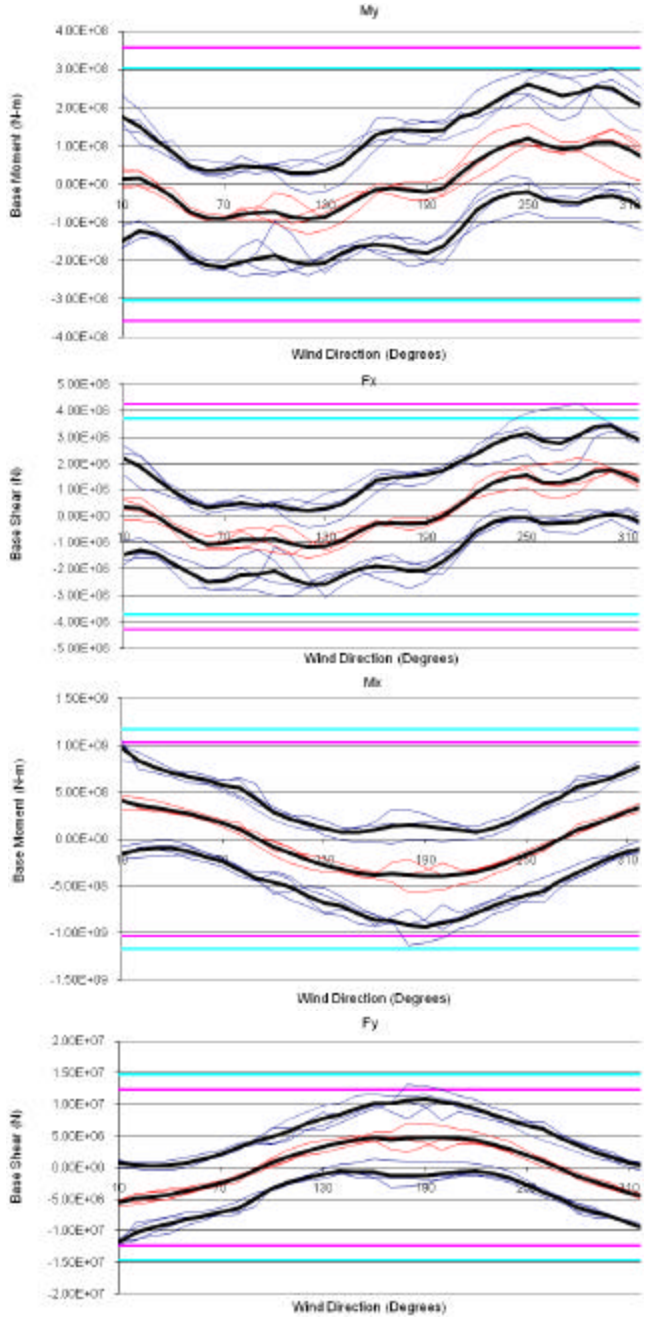

Figure 6. Base moments and shears for rectangular cylinder.

Although a rectangular cylinder closely resembles a square cylinder in shape, the azimuthal force plots for the rectangular section shown in Figure 6 are drastically different from those presented in Figure 3 for a square section. Peak dynamic lift moments caused by vortex shedding, which were evident on the square cylinder were not present in the results for the rectangular cylinder. Furthermore, the code provisions did an excellent job predicting the base wind loads.

The base loads calculated from the factored wind tunnel response of the elliptical seeds can be seen in Figure 7.

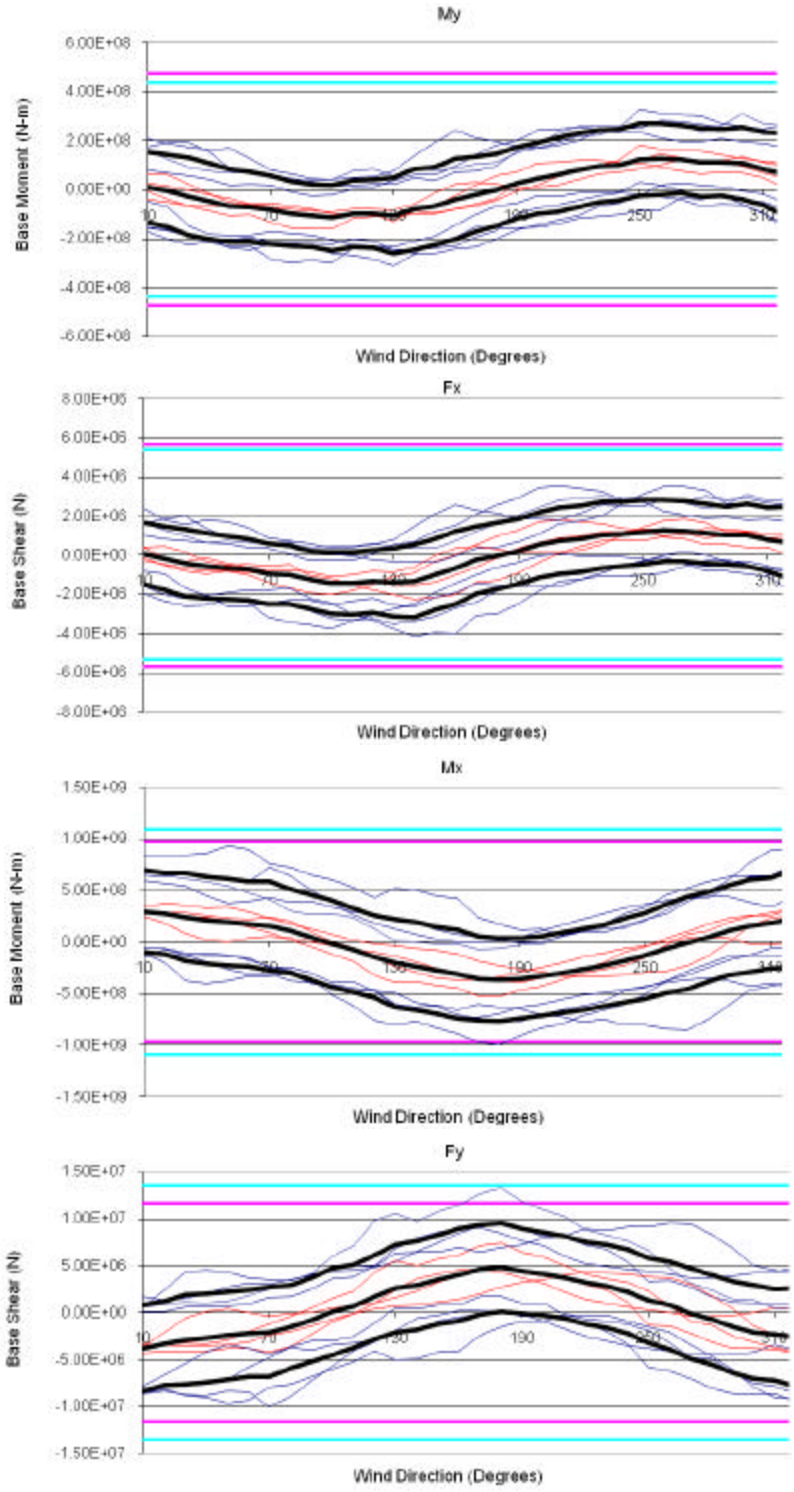

Figure 7. Base moments and shears for elliptical cylinder.

Figure 7 illustrates that the wind loads experienced by the elliptical cylinder in the X-direction (F_x, M_y) are significantly less than the code wind loads. The drag coefficient for an ellipse in the X-direction gives an indication that the wind load experienced by the elliptical cylinder will be considerably less than that calculated for a rectangle. Since the code provisions assume a rectangular section, it seems logical that the X-direction loads on an ellipse would be less than the code predictions. Again, this presents an opportunity for savings through the utilization of BLWT testing. The Y-direction loads (F_y, M_x) fall in line with the code values. High dynamic loads caused by vortex induced oscillation were not apparent in any of the plots in Figure 7.

For design conditions where torsional loads are critical, the torsional eccentricity gives an indication as to how effective a building shape is in reducing torsional loading. The torsion eccentricity is a function of the torsional moment, M_z, the peak base shear, S, and the maximum projected building width, with the relationship shown as Eq. (13).

$$e = \frac{M_z}{\hat{S} \cdot \hat{B}} \tag{13}$$

The torsional eccentricity was calculated for all sample seeds and averaged across each study shape. The average torsion offset for each of the researched shapes is presented in Table 2.

Table 2. Torsional eccentricity for study shapes.

Shape	Torsional Eccentricity
Square	8.3%
Circle	4.0%
Triangle	15.4%
Rectangle	11.4%
Ellipse	10.7%

Table 2 clearly shows that the circular buildings are very effective at reducing torsional loads. Of course, a truly circular building cannot develop any torsional loading about its central axis. Any torsional loads measured on a circular building would be the result of asymmetric surrounding buildings or dynamic loads due to an offset center of mass. Since the center of mass was fixed at the geometric center for this study, the observed torsional loads can be attributed to the presence of unique surrounding buildings adjacent to each of the sample seeds, which produced nominal torsional excitation.

The square seed buildings generated a torsion offset two times greater than that of the circular cylinder. Greater still are the torsion loads generated by the elliptical and rectangular sections, which was to be expected given the wider building dimension in the projected Y-direction. Thus, if reducing torsion loads or torsional velocities is critical for the design of structure, using a circular or square footprint over a elliptical or rectangular floor plan would be advised. Finally, Table 2 shows the high torsion offset present in the triangular section. The torsion offset for the triangular shape exceeded that of all other studied shapes, making the triangular section a poor choice for torsion-sensitive structures.

CONCLUSIONS

The results described above outline the general wind loading characteristics of simplistic building shapes. The data indicate certain shapes that are prone to wind phenomena, such as vortex-shedding, which can generate high dynamic loads and govern the design. Elliptical, triangular and rectangular shaped buildings were identified as being more susceptible to high torsion loading. While the methods presented in the paper are not intended for the determination of design wind loads, it is believed that the general wind loading

patterns illustrated by the authors will be useful in building design circles. It is hoped that this modest research will ignite an interest on the use of aerodynamic shapes and the consideration of building shape, in terms of wind performance, early in the design process.

The intention of the current paper was to focus on shape effects. However, future research could include exploring the sensitivity of each shape to the dynamic properties of the structure (i.e. mass, stiffness, damping). Furthermore, the study could be expanded to include other shapes, such as L-shaped and Y-shaped buildings, buildings with chamfered corners or structures with particular aspect ratios.

ACKNOWLEDGEMENTS

The authors would gratefully acknowledge RWDI group of companies for access to their extensive database of BLWT test data.

REFERENCES

1. American Society of Civil Engineers. 2005. "ASCE 7-05 Standard Minimum Design Loads for Buildings and Other Structures". Reston, Virginia.
2. Boggs, D.W., and J.A. Peterka. 1989. "Aerodynamic model tests of tall buildings". Journal of Engineering Mechanics. 115 (3), 618-635.
3. Brazil, A., L.M. Joseph, D. Poon, and T. Scarangelo. 2006. "Designing High Rises for Wind Performance". ASCE: Structures Congress 2006.
4. Breukelman, B, and Haskett, T. (2001). "Good Vibrations". Civil Engineering. ASCE: Dec. 2001.
5. Browne, M. Suresh Kumar, K. 2005. "Effect of Corner Balconies on Wind-Induced Response of Tall Buildings". The 10th Americas Conference on Wind Engineering. Baton Rouge, Louisiana.
6. Chan C.M., J.K.L Chu, and M.F. Huang. 2009. "Integrated Aerodynamic Load Determination and Stiffness Design Optimization of Tall Buildings". Structural Design of Tall and Special Buildings. 18, 59-80.
7. Chen, X., and A. Kareem. (2005a). "Validity of Wind Load Distribution based on High Frequency Force Balance Measurements". Journal of Structural Engineering. June 2005, 984-987.
8. Chen, X., and A. Kareem. (2005b). "Dynamic Wind Effects of Buildings with 3D Coupled Modes: Application on High Frequency Force Balance Measurements". Journal of Engineering Mechanics. November 2005, 1115-1125.
9. Davenport, A.G. 1971. "The Response of Six Building Shapes to Turbulent Wind". Philosophical Transactions of the Royal Society of London. 269 (1199), 385-394.
10. Dutton, R., and N. Isyumov. 1990. "Reduction of Tall Building Motion by Aerodynamic Treatments". Journal of Wind Engineering and Industrial Aerodynamics. 36, 739-747.
11. Hayashida, H., and Y. Iwasa. 1990. "Aerodynamic Shape Effects of Tall Building for Vortex Induced Vibration". Journal of Wind Engineering and Industrial Aerodynamics. 33, 237-242.
12. Irwin, P.A. 2008. "Bluff Body Aerodynamics in Wind Engineering". Journal of Wind Engineering and Industrial Aerodynamics. 96, 701-712.
13. Irwin, P., B. Breukelman, C. Williams, and M. Hunter. 1998. "Shaping and Orienting Tall Buildings for Wind". 1st World Structures Congress, San Francisco, CA.
14. Jackson, C.P. 1987. "A Finite-Element Study of the Onset of Vortex Shedding in Flow Past Variously Shaped Bodies". Journal of Fluid Mechanics. 182, 23-45.
15. Kareem, A. 1992. "Dynamic Response of High-Rise Buildings to Stochastic Wind Loads". Journal of Wind Engineering and Industrial Aerodynamics. 41-44, 1101-1112.
16. Kareem, A. 1983. "Mitigation of Wind Induced Motion of Tall Buildings". Journal of Wind Engineering and Industrial Aerodynamics. 11, 273-284.
17. Kawai, H. 1998. "Effect of Corner Modifications on Aeroelastic Instabilities of Tall Buildings". Journal of Wind Engineering and Industrial Aerodynamics. 74-76, 719-729.

18. National Research Council of Canada - Institute of Research in Construction. 2005. "National Building Code of Canada". Ottawa, Ontario.
19. Newmark, N., and W. Hall. 1982. "Earthquake Spectra and Design". Earthquake Engineering and Research Institute.
20. Merrick, R. and G. Bitsuamlak, G.T. (2008) "Control of flow around a circular cylinder by the use of surface roughness: A computational and experimental approach", 4th International Conference on Advances in Wind and Structures (AWAS08), May 2008, Jeju, Korea.
21. Simiu, E., and T. Miyata. 2006. "Design of Buildings and Bridges for Wind". John Wiley & Sons, New Jersey. Simiu, E., and R. Scanlan. 1996. "Wind Effects on Structures". John Wiley & Sons, New York.
22. Tamura, T., and T. Miyagi. 1999. "The Effect of Turbulence on Aerodynamic Forces on a Square Cylinder with Various Corner Shapes". Journal of Wind Engineering and Industrial Aerodynamics. 83, 135-145.
23. Tschanz, T., and A. G. Davenport. 1983. "The Base Balance Technique for the Determination of DynamicWind Loads". Journal of Wind Engineering and Industrial Aerodynamics. 13, 429-439.
24. Xie, J., and P.A. Irwin. 1998. "Application of Force Balance Technique to a Building Complex". Journal of Wind Engineering and Industrial Aerodynamics. 77&78, 579-590.
25. Zhou, Y., T. Kijewski, and A. Kareem. 2003. "Aerodynamic Loads on Tall Buildings: Interactive Data base". Journal of Structural Engineering. ASCE: March 2006, 394-404.

APPENDIX A. Seed Building Information.

Footprint	Height (m)	Max. Width (m)	Aspect Ratio	Slenderness Ratio
	242	34	1.02	7.26
	264	34	1.00	7.76
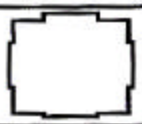	278	35	1.00	7.94
	148	29	1.18	6.02
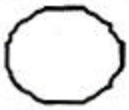	262	58	1.00	4.52
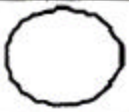	102	13	1.00	7.85
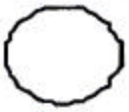	156	40	1.00	3.90
	96	10	1.00	9.60
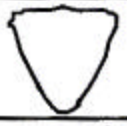	350	56	1.20	7.50
	235	60	1.08	4.23

APPENDIX A. Seed Building Information (cont'd).

Footprint	Height (m)	Max. Width (m)	Aspect Ratio	Slenderness Ratio
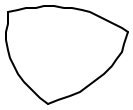	174	45	1.05	4.06
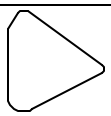	67	35	1.23	2.35
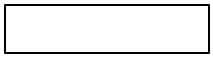	98	77	3.35	4.26
	121	67	2.23	4.02
	193	82	2.33	5.48
	100	41	1.83	4.46
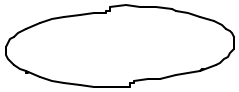	107	100	2.37	2.54
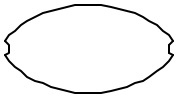	96	48	1.53	3.06
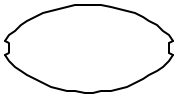	96	48	1.53	3.06
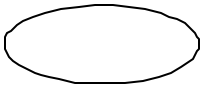	120	49	1.99	4.87